COMMUNICATION

CrossMark
click for updates

Nitrate uptake using mesoporous silica embedded with zero-valent palladium nanoparticles†

Chee Ling Tong,[a] Ela Eroglu,[bc] Xiaofei Duan,[d] Robert N. Lamb,[d] Kevin Jarrett,[e] Craig E. Buckley[e] and Colin L. Raston*[a]

In situ reduction of palladium(II) acetylacetonate during the synthesis of SBA-15 mesoporous silica affords a material impregnated with palladium nanoparticles. The synthesis is at neutral pH and ambient conditions using a continuous flow vortex fluidic device with high shear dynamic thin films, followed by calcination. The SBA-15 is available with considerably reduced processing time relative to the conventional synthesis of mesoporous silica, with the material being effective for nitrate-nitrogen [NO_3^--N] removal from aqueous solutions, at 41% within the first 16 hours, or around 36% for the same period after being recycled.

SBA-15 is a mesoporous silica prepared using a non-ionic amphiphilic copolymer template,[1] possessing novel physical characteristics and hydrothermal stability. Well defined pores in the material relate to its application in catalysis, separation science, drug delivery, and biosensors.[2–4] Advances have been made in improving the synthesis with finer control on the structure and morphology of the material.[5–9] Most of the focus has been on the chemistry, as in functionalizing the material,[10] or adding swelling agents for pore expansion.[11–13] Nonetheless, the synthesis follows the conventional hydrothermal process, which typically takes 48 hours for an individual batch, and reducing this time has been challenging. To this end, we recently made progress in reducing the processing time, using a vortex fluidic device (VFD) for the pre-calcining stage, where the

reactions are under shear and are not diffusion controlled.[14] Indeed there is limited literature on the synthesis of silica involving such external shear enhancement. Amorphous silica has been prepared using shear flow in a Couette cell under neutral conditions, albeit without much detail provided on the characterization of the material.[15] Kim *et al.* prepared mesoporous silica involving shear flow in a Couette cell operating under laminar flow conditions, although this involved multiple steps and different operating temperatures.[16] The aforementioned synthesis of SBA-15 using a VFD under ambient conditions,[14] significantly reduced the processing time to *ca.* 5 hours, prior to the calcination step. Here the turbulent shear condition within the device circumvents the need for hydrothermal aging.[14] The simplicity of the VFD processing approach offers scope for customizing the synthesis, depending on the target application, for example nitrate remediation, which is the focus herein.

Heavy usage of artificial fertilizers has resulted in nitrate contamination of ground and surface water.[17] The standard regulations for nitrate-nitrogen concentration [NO_3^--N] in drinking water is less than 10 mg L^{-1}.[18] Nitrate removal has been established for a number of techniques, including ion exchange, biological denitrification,[19,20] electro-reduction and electro-coagulation,[17] chemical denitrification, reverse osmosis, electrodialysis, and catalytic denitrification.[21] Among these commonly used treatment methods, they all have the disadvantage of requiring post-treatment.[22] This can be overcome using desorption methods.[22] Adsorbents such as activated carbon, sepiolite, and slag have been studied in nitrate removal.[23] However, much attention has been devoted to the performance of low cost readily materials such as tree bark, wood charcoal, saw dust, alum sludge, and red mud.[24] There are also studies on the catalytic reduction of nitrate using palladium based catalyst and hydrogen gas as the reducing agent, but they have been limited to bench-scale processing. This relates to technical challenges such as catalytic fouling.[25] Combining two approaches of utilizing an adsorption method followed by a hydrodeoxygenation reaction would be

[a] Flinders Centre for NanoScale Science and Technology, School of Chemical and Physical Sciences, Flinders University, Bedford Park, SA 5042, Australia. E-mail: colin.raston@flinders.edu.au

[b] School of Chemistry and Biochemistry, The University of Western Australia, Crawley, WA 6009, Australia

[c] ARC Centre of Excellence in Plant Energy Biology, The University of Western Australia, Crawley, WA 6009, Australia

[d] Surface and Chemical Analysis Network, School of Chemistry, The University of Melbourne, Parkville, Victoria 3010, Australia

[e] Department of Imaging and Applied Physics, Fuels and Energy Technology Institute, Curtin University, GPO Box U1987, Perth 6845, WA, Australia

advantageous. Incorporating palladium in SBA-15 as an adsorbent offers scope for recovery and recycling of the material while avoiding fouling of the catalyst. In the present study we report the *in situ* synthesis of SBA-15 loaded with zero-valent palladium nanoparticles, and the utility of the material in the removal of nitrate from waste effluent. The reduced palladium nanoparticles provide an active site for catalytic reduction of nitrate *via* hydrodeoxygenation.[25] To our knowledge there are no reports on the use of Pd/SBA-15 as an adsorbent for nitrate removal.

The synthesis herein involves the use of the VFD for the *in situ* incorporation of metal nanoparticles within the pores of SBA-15 using a Pd(II) precursor. We recently reported a detailed study of the synthesis of SBA-15 using the VFD under acidic and ambient conditions, establishing the ability to control the pore size over a range of operating conditions.[14] In a related study we used the VFD to prepare mesoporous silica in the absence of a copolymer, for direct impregnation of particles of an anti-microbial compound into the material, at neutral pH and under ambient conditions, for controlled release at physiological pH.[26] These findings form the basis of the present study, with now a focus on gaining access to an adsorbent material for nitrate removal. Here the synthesis is carried out under neutral pH which enables direct deposition of metal oxide, in the presence of a copolymer template.

The synthesis of SBA-15 impregnated with Pd(0) nanoparticles is as follows: 2.5 g of Pluronic® P-123 was dissolved in 50 mL of deionized water at 40–45 °C and 100 mg of palladium(II) acetylacetonate [Pd(acac)$_2$] was added to the resulting micelle solution. The mixture was fed into the VFD, Fig. 1, at a flow rate of 0.5 mL min^{-1} with the 18.0 mm internal diameter (20.0 mm external diameter) borosilicate glass tube (as a standard NMR tube) spun at 5000 rpm at a tilt angle of 45°. Then 0.375 mL of 0.5 M aqueous sodium fluoride (NaF) was added to the resulting pre-stressed Pd(II)/P-123 mixture, and the solution was fed back into the VFD through one jet-1, with 4.0 mL of tetramethoxysilane (TMOS) simultaneously fed into the VFD through a second jet feed-2. The VFD operating condition were also at 5000 rpm and 45° tilting angle, but now under a H$_2$/N$_2$ atmosphere, with the hydrogen for reducing Pd(II). Detailed synthetic procedures can be found in the ESI.† The overall processing time of the synthesis was 5 hours, with the residence time of a finite volume of liquid in the tube at *ca.* 3 minutes (Fig. 1). The resulting materials were then calcined at 550 °C under H$_2$ for 6 hours, to remove the polymer template. Initially we used H$_2$PdCl$_4$ in 35% aqua regia as the palladium precursor and synthesize the Pd/SBA-15 using the same synthetic approach under acidic conditions, but the resulting product did not show high mesoregularity, with the palladium particles agglomerated rather than monodispersed inside the channels. In addition, the surface morphology of the material established from scanning electron microscopy (SEM) and transmission electron microscopy (TEM) images suggests incomplete condensation using H$_2$PdCl$_4$ precursor (ESI Fig. S1†).

A small angle X-ray scattering (SAXS) pattern of the calcined material was collected and a strong diffraction peak for the (1 0 0) plane appeared at $q = 0.0555 \pm 0.0014$ Å^{-1} (Fig. S2†),
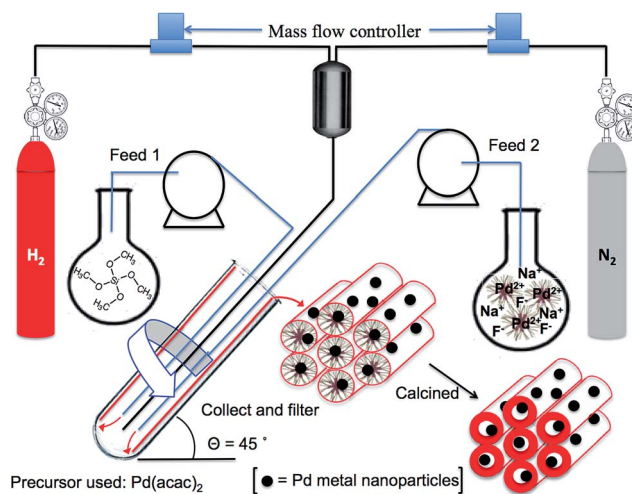

Fig. 1 Schematic of the continuous synthesis of Pd/SBA-15 using a vortex fluidic device (VFD).

which corresponds to a *d*-spacing of 113.2 ± 2.86 Å (Table S1†) and a unit cell parameter, a_o of 130.7 ± 3.30 Å (Fig. S3†). No obvious secondary diffraction of (1 1 0) and (2 0 0) plane were observed in the sample. These second order peaks will be washed out by Guinier features (from the size of the Pd particles) causing a decrease in scattering contrast between the pore walls and the pore channels when palladium nanoparticles are incorporated inside the pores.[27] This is proven by comparing the SAXS patterns of SBA-15 and Pd/SBA-15 (Fig. S3†).

The surface area, pore volume and pore diameter of the heterogeneous catalyst were investigated using nitrogen adsorption–desorption. The calcined material exhibits a typical type IV isotherm with H1 hysteresis loop according to IUPAC classification (Fig. 2), indicating a uniform mesostructure and cylindrical channels.[28] The step increase at relative pressure around 0.45–0.5 was attributed to the capillary condensation of N$_2$ into the mesopores. The material has a Brunauer–Emmett–Teller (BET) surface area of 700.1 m^2 g^{-1} and pore volume of 0.76 cm^3 g^{-1}. The narrow pore size distribution of the
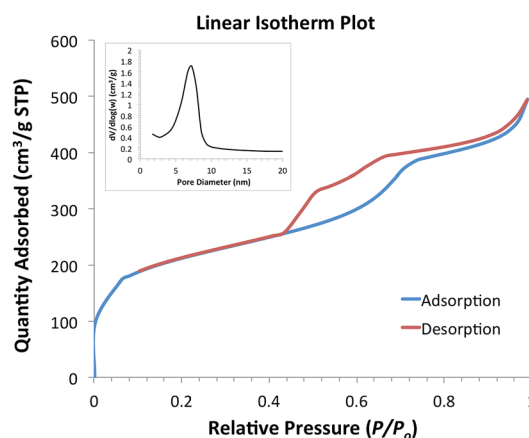

Fig. 2 N$_2$ adsorption–desorption of Pd/SBA-15 and the pore size distribution of the adsorption branch (inset).

adsorption branch (inset of Fig. 2) according to Barrett–Joyner–Halenda (BJH) method was centred at 5.4 nm.

SEM images showed the formation of short-chain like sections interconnected throughout, Fig. 3(a). Energy-dispersive X-ray spectroscopy (EDS) *via* SEM was conducted with a full area scanned and mapped for individual elements, silica (Si), oxygen (O) and palladium (Pd), establishing the presence of the elements (Fig. S4†). Inductively coupled plasma mass spectrometry (ICP-MS) gave 1.53 wt% of palladium content in the calcined material, which impart high palladium incorporation, at 81%, into the final product. Transmission electron microscopy (TEM) revealed the inner pore structure of the material, showing a well-ordered mesostructure with estimated pore diameter around 5.5–6 nm which was close to the average pore diameter reported using the BJH method based on N_2 adsorption–desorption analysis. Palladium nanoparticles (PdNPs) were revealed as darker contrast regions in the TEM images, with estimated diameters of ~4–5 nm, and are embedded within the pore channels (Fig. 3(b)). Ruas *et al.* utilized an alcohol reduction method to prepare a suspension of Pd(0) solution using $Pd(acac)_2$ as the metal precursor, and poly-vinylpyrrolidone (PVP) as a stabilizer, with a particle size distribution at 5.8 ± 1.1 nm, which agrees with our finding.[29] In addition, using palladium(II) hexafluoroacetylacetonate $[Pd(hfac)_2]$ as precursor, the Pd crystallite sizes impregnated into SBA-15 range from 6.0 to 7.9 nm, and the post deposition required 3 to 8 hours under supercritical carbon dioxide (scCO₂).[30] The size of the PdNPs formed inside the channels is likely to vary with different precursors as well as the choice of solvent system. This is based on their important role in controlling the nucleation and growth of PdNPs.[29,31,32]

As mentioned above, the synthesis was carried out under H_2 to act as a reducing agent in forming elemental palladium nanoparticles. X-ray photoelectron spectroscopy (XPS) was performed to ascertain the oxidation state of the element in the final sample. Survey scans were carried out over the binding energy range 0–1200 eV with 1.0 eV step size and 100 ms dwell time, but no visible Pd peak was observed. Since most of the palladium nanoparticles were clearly incorporated inside the pore channels, an argon ion beam was used to etch the silica surface. A crater area of 3×3 mm with approximately 18 nm of the surface layer being sputtered off, was investigated by high resolution scans at analyzer pass energies of 50 eV. The peaks of $Pd3d_{5/2}$ and $Pd3d_{3/2}$ binding energy at 335.7 eV and 341.0 eV were observed by deconvolution, indicating an oxidation state of Pd(0) (Fig. S5†).
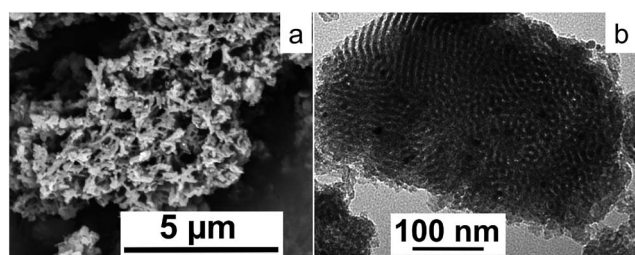
Fig. 4 shows the amount of NO_3^--N concentration of the aqueous media at various time intervals, after being exposed to Pd/SBA-15 samples. Initially, the NO_3^--N concentration in the untreated aqueous media was 23 mg L^{-1}. The increase in the amount of adsorbent loading had an affirmative effect on the amount of nitrate-nitrogen adsorbed from the liquid media. All of these three loading capacities achieved their maximal nitrate removal efficiencies after 16 hours, which stabilized thereafter. As shown in Fig. 4, 50 mg of adsorbent yielded the highest nitrate-nitrogen adsorption value of 9.5 mg L^{-1} (41% removal efficiency of the initial value), which was followed by 8.0 mg L^{-1} adsorption (35% removal efficiency) by the 25 mg sample, and 6.5 mg L^{-1} adsorption (28% removal efficiency) by the 10 mg sample. The control experiment with only-silica samples was also investigated using the same amount of adsorbent loadings, with little nitrate removed. This also confirms that the zero valence palladium nanoparticles of the sample are responsible for the nitrate removal. In this context, palladium metal, either monometallic or bimetallic forms, notably Pd–Cu, Pd–Sn or Pd–In, are effective catalysts for the adsorption and catalytic reduction of nitrate.[18]

From Fig. 4, both 10 mg and 25 mg samples followed a first order adsorption kinetics for the nitrate-nitrogen removal within the first 16th hour, yielding adsorption rates of around 0.4 mg L^{-1} h^{-1} NO_3^--N (~1.8 mg L^{-1} h^{-1} NO_3^-) and 0.5 mg L^{-1} h^{-1} NO_3^--N (~2.2 mg L^{-1} h^{-1} NO_3^-), respectively. On the other hand, the most concentrated sample (50 mg adsorbent) followed a different adsorption pattern than the other samples, and showed separate removal rates for the time periods of 0–4 h and 8–16 h, resulting in nitrate-nitrogen removal rates of approximately 1.3 mg L^{-1} h^{-1} NO_3^--N (~5.8 mg L^{-1} h^{-1} NO_3^-) and 1.1 mg L^{-1} h^{-1} NO_3^--N (~4.9 mg L^{-1} h^{-1} NO_3^-), respectively. The kinetic calculations and the accuracy of the removal rates can be improved by measuring more data points within shorter time intervals, which is possible in a larger scale experiment using higher volumes of effluent. While still on the slower side, these nitrate-nitrogen removal rates of the current
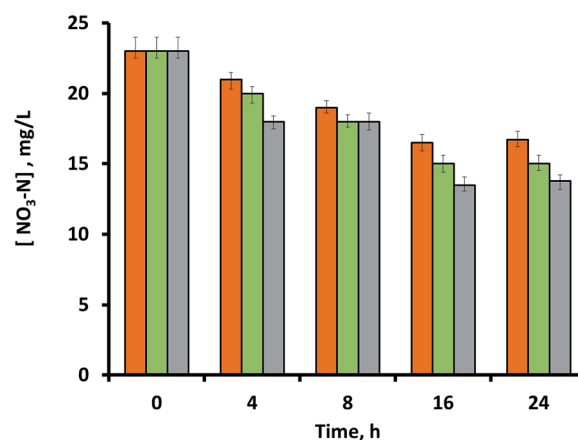

Fig. 3 (a) SEM image of Pd/SBA-15 and (b) TEM image of Pd/SBA-15.

Fig. 4 Nitrate-nitrogen $[NO_3^-$-N] content of aqueous media in mg L^{-1} *versus* time for three different Pd/SBA-15 loading concentrations: (1) 10 mg adsorbent (brown column); (2) 25 mg adsorbent (green column); and (3) 50 mg adsorbent (grey column).

Table 1 Nitrate-nitrogen [NO_3^--N] removal efficiencies of Pd/SBA-15 by two consecutive cycles[a]

[NO_3^--N] removal efficiencies (mg L^{-1})	Amount of Pd/SBA-15		
	10 mg	25 mg	50 mg
1st cycle, maximum [NO_3^--N] removal[b]	6.5 ± 0.6	8.0 ± 0.6	9.5 ± 0.5
2nd cycle, maximum [NO_3^--N] removal[b]	4.5 ± 0.3	6.5 ± 0.4	8.2 ± 0.4
Total [NO_3^--N] removal for two consecutive batches[c]	11.0 ± 0.7	14.5 ± 0.7	17.7 ± 0.6

[a] The numbers given here represent the amount of nitrate-nitrogen [NO_3^--N] ions removed from the solution, rather than the amount present in the solution. [b] Errors reported were deviations from the mean. [c] Reported overall errors for each batch are calculated using the standard error propagation formula.

study are relatively comparable with those reported in the literature on monometallic-palladium containing adsorbents, although it is difficult to make a direct comparison within those studies due to the large variations among the experimental parameters such as the variations in the nitrate removal mechanism, composition and type of the adsorbent, amount of other reducing agents such as catalytic hydrogen, initial concentration and the presence of other ions in the nitrate containing effluent, the scale of the process, and more. As an example, catalytic processes with monometallic palladium reported by Devadas *et al.* had a nitrate removal rate of ~4.2 mg L^{-1} h^{-1} NO_3^- with Pd on a support of ceria (CeO_2) under the flow of 80% H_2 + 20% CO_2 gas. They also found that significantly high nitrate removal rate was achieved with the same Pd/CeO_2 catalyst under pure hydrogen flow, reaching a value of around 46.5 mg L^{-1} h^{-1} NO_3^-.[33]

Based on the results shown in Fig. 4, 16 hours was chosen as the optimal time-interval for testing the recycling potential of the adsorbent. Here, used samples were washed with deionized water through hand-vortexing for 1 minute, followed by removal of the supernatant after centrifugation at 9390 × *g* for 5 minutes. Remaining samples were then mixed again with nitrate-containing fresh media (1.5 mL), while the final nitrate-nitrogen content of the second batch was analyzed after 16 hours of that cycle. Recycling results showed that the Pd/SBA-15 samples were still effective for the removal of nitrate during their second cycle (Table 1), albeit with a slight decrease in their maximum removal efficiencies. The Pd/SBA-15 samples were retrieved and analysed using XPS to investigate if the palladium nanoparticles were oxidized after the treatment. From the spectra, the peaks of Pd3d$_{5/2}$ and Pd3d$_{3/2}$ binding energy at 335.5 eV and 340.7 eV were observed by deconvolution, indicating palladium in its elemental form (Fig. S6†).

Conclusions

An efficient method involving the use of the VFD has been developed for preparing mesoporous silica loaded with elemental palladium nanoparticles at neutral pH. This material is effective in wastewater treatment in targeting nitrate-nitrogen removal, showing a maximum nitrate-nitrogen removal efficiency of 41% after 16 hours. Recyclability of the same adsorbent was examined, establishing a 36% maximum nitrate-nitrogen removal efficiency. While this is lower, it

nevertheless is promising given that Pd/SBA-15 can be easily separated from the liquid effluent.

The novel processing technology of VFD has the advantages of operating under ambient conditions and having a five-fold reduction in processing time relative to the synthesis of conventional hydrothermal processed SBA-15. Also noteworthy is the inherent cost savings in the production of SBA-15 and the analogous material loaded with palladium nanoparticles. This is potentially attractive to industry, as is the ability to generate metal nanoparticles almost exclusively embedded in the pores of the material, rather than on the surface, thereby minimising different outcomes for particles in different environments. This work further highlights the growing applications of the VFD, which also includes its ability to refold protiens.[34]

Notes and references

1 D. Zhao, J. Feng, Q. Huo, N. Melosh, G. H. Fredrickson, B. F. Chmelka and G. D. Stucky, *Science*, 1998, **279**, 548–552.
2 J. r. P. Thielemann, F. Girgsdies, R. Schlögl and C. Hess, *Beilstein J. Nanotechnol.*, 2011, **2**, 110–118.
3 L. Y. Chen, S. Jaenicke and G. K. Chuah, *Microporous Mater.*, 1997, **12**, 323–330.
4 S. Lin, L. Shi, M. M. L. Ribeiro Carrott, P. J. M. Carrott, J. Rocha, M. R. Li and X. D. Zou, *Microporous Mesoporous Mater.*, 2011, **142**, 526–534.
5 D. Zhao, Q. Huo, J. Feng, B. F. Chmelka and G. D. Stucky, *J. Am. Chem. Soc.*, 1998, **120**, 6024–6036.
6 R. Ryoo, C. H. Ko, M. Kruk, V. Antochshuk and M. Jaroniec, *J. Phys. Chem. B*, 2000, **104**, 11465–11471.
7 D. Zhao, J. Sun, Q. Li and G. D. Stucky, *Chem. Mater.*, 2000, **12**, 275–279.
8 H. I. Lee, J. H. Kim, G. D. Stucky, Y. Shi, C. Pak and J. M. Kim, *J. Mater. Chem.*, 2010, **20**, 8483–8487.
9 Y. Wan and D. Zhao, *Chem. Rev.*, 2007, **107**, 2821–2860.

10 D. Margolese, J. A. Melero, S. C. Christiansen, B. F. Chmelka and G. D. Stucky, *Chem. Mater.*, 2000, **12**, 2448–2459.

11 P. Schmidt-Winkel, W. W. Lukens, D. Zhao, P. Yang, B. F. Chmelka and G. D. Stucky, *J. Am. Chem. Soc.*, 1998, **121**, 254–255.

12 J. S. Lettow, Y. J. Han, P. Schmidt-Winkel, P. Yang, D. Zhao, G. D. Stucky and J. Y. Ying, *Langmuir*, 2000, **16**, 8291–8295.

13 L. Cao and M. Kruk, *Colloids Surf., A*, 2010, **357**, 91–96.

14 C. L. Tong, R. A. Boulos, C. Yu, K. S. Iyer and C. L. Raston, *RSC Adv.*, 2013, **3**, 18767–18770.

15 S. Patwardhan, N. Mukherjee and S. Clarson, *J. Inorg. Organomet. Polym.*, 2001, **11**, 117–121.

16 W.-J. Kim and S.-M. Yang, *Chem. Mater.*, 2000, **12**, 3227–3235.

17 A. S. Koparal and Ü. B. Öğütveren, *J. Hazard. Mater.*, 2002, **89**, 83–94.

18 Y. Wang, J. Qu, H. Liu and C. Hu, *Catal. Today*, 2007, **126**, 476–482.

19 E. Eroglu, V. Agarwal, M. Bradshaw, X. Chen, S. M. Smith, C. L. Raston and K. Swaminathan Iyer, *Green Chem.*, 2012, **14**, 2682–2685.

20 M. H. Wahid, E. Eroglu, X. Chen, S. M. Smith and C. L. Raston, *Green Chem.*, 2013, **15**, 650–655.

21 A. Kapoor and T. Viraraghavan, *J. Environ. Eng.*, 1997, **123**, 371–380.

22 A. Bhatnagar and M. Sillanpää, *Chem. Eng. J.*, 2011, **168**, 493–504.

23 N. Öztürk and T. E. Bektaş, *J. Hazard. Mater.*, 2004, **112**, 155–162.

24 Y. Cengeloglu, A. Tor, M. Ersoz and G. Arslan, *Sep. Purif. Technol.*, 2006, **51**, 374–378.

25 B. P. Chaplin, M. Reinhard, W. F. Schneider, C. Schüth, J. R. Shapley, T. J. Strathmann and C. J. Werth, *Environ. Sci. Technol.*, 2012, **46**, 3655–3670.

26 C. L. Tong, U. H. Stroeher, M. H. Brown and C. L. Raston, *RSC Adv.*, 2015, **5**, 7953–7958.

27 A. Martin, G. Morales, F. Martinez, R. van Grieken, L. Cao and M. Kruk, *J. Mater. Chem.*, 2010, **20**, 8026–8035.

28 R. Che, D. Gu, L. Shi and D. Zhao, *J. Mater. Chem.*, 2011, **21**, 17371–17381.

29 C. P. Ruas, D. K. Fischer and M. A. Gelesky, *J. Nanotechnol.*, 2013, **2013**, 6.

30 J. Morère, M. J. Tenorio, M. J. Torralvo, C. Pando, J. A. R. Renuncio and A. Cabañas, *J. Supercrit. Fluids*, 2011, **56**, 213–222.

31 S. Yang, J. Dong, Z. Yao, C. Shen, X. Shi, Y. Tian, S. Lin and X. Zhang, *Sci. Rep.*, 2014, **4**, 4501.

32 L. Zhang, L. Wang, Z. Jiang and Z. Xie, *Nanoscale Res. Lett.*, 2012, **7**, 312.

33 A. Devadas, S. Vasudevan and F. Epron, *J. Hazard. Mater.*, 2011, **185**, 1412–1417.

34 T. Z. Yuan, C. F. G. Ormonde, S. T. Kudlacek, S. Kunche, J. N. Smith, W. A. Brown, K. M. Pugliese, T. J. Olsen, M. Iftikhar, C. L. Raston and G. A. Weiss, *ChemBioChem*, 2015, **16**, 393–396.